Eur. Phys. J. C (2019) 79:537
https://doi.org/10.1140/epjc/s10052-019-6698-3

THE EUROPEAN PHYSICAL JOURNAL C

Regular Article - Experimental Physics

Measurement of the branching fraction and *CP* asymmetry in $B^+ \to J/\psi\,\rho^+$ decays

LHCb Collaboration[⋆]

CERN, 1211, Geneva 23, Switzerland

Received: 20 December 2018 / Accepted: 15 February 2019

Abstract The branching fraction and direct *CP* asymmetry of the decay $B^+ \to J/\psi\,\rho^+$ are measured using proton-proton collision data collected with the LHCb detector at centre-of-mass energies of 7 and 8 TeV, corresponding to a total integrated luminosity of $3\,\text{fb}^{-1}$. The following results are obtained:

$$\mathcal{B}(B^+ \to J/\psi\,\rho^+) = (3.81^{+0.25}_{-0.24} \pm 0.35) \times 10^{-5},$$
$$\mathcal{A}^{CP}(B^+ \to J/\psi\,\rho^+) = -0.045^{+0.056}_{-0.057} \pm 0.008,$$

where the first uncertainties are statistical and the second systematic. Both measurements are the most precise to date.

1 Introduction

In the Standard Model of particle physics, the decay $B^+ \to J/\psi\,\rho^+$ proceeds predominantly via a $b \to c\bar{c}d$ transition involving tree and penguin amplitudes,[1] as shown in Fig. 1. Interference between these two amplitudes can lead to direct *CP* violation that is measured through an asymmetry defined as

$$\mathcal{A}^{CP} \equiv \frac{\mathcal{B}(B^- \to J/\psi\,\rho^-) - \mathcal{B}(B^+ \to J/\psi\,\rho^+)}{\mathcal{B}(B^- \to J/\psi\,\rho^-) + \mathcal{B}(B^+ \to J/\psi\,\rho^+)}. \quad (1)$$

No precise prediction for $\mathcal{A}^{CP}$ exists, though it is expected to have an absolute value $\lesssim 0.35$ [1] assuming isospin symmetry between the $B^0 \to J/\psi\,\rho^0$ and the $B^+ \to J/\psi\,\rho^+$ decays. Measurements of $\mathcal{A}^{CP}$ provide an estimate of the imaginary part of the penguin-to-tree amplitude ratio for the $b \to c\bar{c}d$ transition. Similarly to the $B^0 \to J/\psi\,\rho^0$ decay [2], the *CP* asymmetry is expected to be enhanced in this decay compared to the decay $B_s^0 \to J/\psi\,\phi$ [3,4]. Therefore its value can be used to place constraints on penguin effects in measurements of the *CP*-violating phase ϕ_s from the decay $B_s^0 \to J/\psi\,\phi$, assuming approximate SU(3) flavour symmetry and neglecting exchange and annihilation diagrams. The branching fraction and the value of $\mathcal{A}^{CP}$ for $B^+ \to J/\psi\,\rho^+$ decays were measured previously by the BaBar collaboration to be $(5.0 \pm 0.7 \pm 0.3) \times 10^{-5}$ and $-0.11 \pm 0.12 \pm 0.08$, respectively [5].

In this paper, the branching fraction and the direct *CP* asymmetry of the decay $B^+ \to J/\psi\,\rho^+$ are measured using proton-proton (pp) collision data collected with the LHCb detector at centre-of-mass energies of 7 TeV (in 2011) and 8 TeV (in 2012), corresponding to a total integrated luminosity of $3\,\text{fb}^{-1}$. The $B^+ \to J/\psi\,\rho^+$ decay is analysed using the $J/\psi \to \mu^+\mu^-$, $\rho^+ \to \pi^+\pi^0$ and $\pi^0 \to \gamma\gamma$ decays. Its branching fraction is measured relative to that of the abundant decay $B^+ \to J/\psi\,K^+$, which has the same number of charged final-state particles and contains a J/ψ meson as the decay of interest.

2 Detector and simulation

The LHCb detector [6,7] is a single-arm forward spectrometer covering the pseudorapidity range $2 < \eta < 5$, designed for the study of particles containing b or c quarks. The detector includes a high-precision tracking system consisting of a silicon-strip vertex detector surrounding the pp interaction region [8], a large-area silicon-strip detector located upstream of a dipole magnet with a bending power of about 4 Tm, and three stations of silicon-strip detectors and straw drift tubes [9] placed downstream of the magnet. The tracking system provides a measurement of the momentum, p, of charged particles with a relative uncertainty that varies from 0.5% at low momentum to 1.0% at 200 GeV/c. The minimum distance of a track to a primary vertex (PV), the impact parameter (IP), is measured with a resolution of $(15 + 29/p_{\text{T}})$ μm, where p_{T} is the component of the momentum transverse to the beam, in GeV/c. Different types of charged hadrons are distinguished using information from

[1] Charge conjugation is implied throughout this paper, unless otherwise stated.

[⋆] e-mail: michel.de.cian@cern.ch

Published online: 24 June 2019

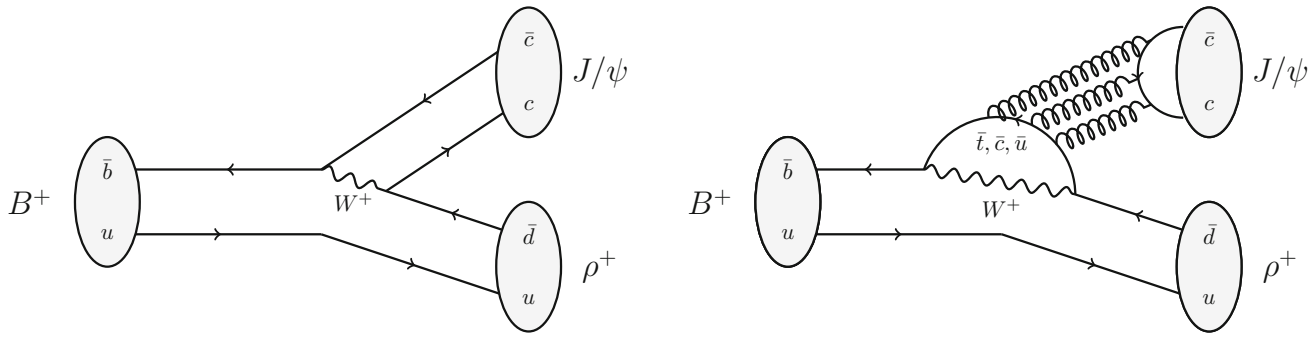

Fig. 1 Leading-order Feynman diagrams for the (left) tree and (right) penguin amplitudes contributing to the decay $B^+ \to J/\psi\,\rho^+$

two ring-imaging Cherenkov (RICH) detectors [10]. Photons, electrons and hadrons are identified by a calorimeter system consisting of scintillating-pad and preshower detectors, an electromagnetic and a hadronic calorimeter. Muons are identified by a system composed of alternating layers of iron and multiwire proportional chambers [11].

The magnetic field deflects oppositely charged particles in opposite directions which can lead to charge-dependent acceptance effects. The configuration with the magnetic field pointing upwards (downwards) bends positively (negatively) charged particles in the horizontal plane towards the centre of the LHC ring. Periodically reversing the magnetic field polarity throughout the data taking sufficiently cancels these acceptance effects for the precision of this measurement. Furthermore, the possible difference in material interactions between positively and negatively charged pions is negligible for this analysis [12].

The online event selection is performed by a trigger [13], which consists of a hardware stage, based on information from the calorimeter and muon systems, followed by a software stage, which applies a full event reconstruction. For this analysis, the hardware trigger requires at least one muon with a transverse momentum larger than 1.5 GeV/c in 2011 and 1.8 GeV/c in 2012. The first stage of the software trigger requires either a muon candidate with a momentum larger than 8 GeV/c and a transverse momentum larger than 1 GeV/c, or two muons that form a good quality vertex with an invariant mass greater than 2.7 GeV/c^2. In the second stage of the software trigger, two particles, identified as being muons, must form a good-quality vertex with an invariant mass compatible with the known J/ψ mass [14].

Simulated events are used to study the kinematical properties of the $B^+ \to J/\psi\,\rho^+$ and $B^+ \to J/\psi\,K^+$ decays, to study the background contamination and to evaluate the selection efficiencies. In the simulation, pp collisions are generated using Pythia [15,16] with a specific LHCb configuration [17]. Decays of hadronic particles are described by EvtGen [18], in which final-state radiation is generated using Photos [19]. The interaction of the generated particles with the detector, and its response, are implemented using the Geant4 toolkit [20,21] as described in Ref. [22].

3 Selection

The same selection criteria are placed on the J/ψ candidates for both decays, $B^+ \to J/\psi\,\rho^+$ and $B^+ \to J/\psi\,K^+$. Each J/ψ candidate is composed of two tracks compatible with being muons that form a good quality common vertex significantly displaced from any reconstructed PV in the event. The invariant mass of this two-track combination must be within ± 100 MeV/c^2 of the known J/ψ mass [14].

For the $B^+ \to J/\psi\,\rho^+$ decay, each ρ^+ candidate is formed from a charged and a neutral pion. The charged pion is required to have a $\chi^2_{\rm IP}$ value that is inconsistent with originating from any PV in the event, where $\chi^2_{\rm IP}$ is defined as the difference between the vertex-fit χ^2 of a given PV reconstructed with and without the particle under consideration. The charged pion also needs to have a momentum larger than 3 GeV/c and a transverse momentum larger than 250 MeV/c. To reject background from $B^+ \to J/\psi\,K^{*+}$ decays,[2] with $K^{*+} \to K^+\pi^0$, where a kaon is misidentified as a pion, a stringent criterion is placed on the pion-identification quality, which is mainly derived using information from the two RICH detectors. The neutral pion is reconstructed from two well-separated clusters in the electromagnetic calorimeter. It is required to have a $p_{\rm T}$ larger than 800 MeV/c. The ρ^+ candidate must have a transverse momentum larger than 800 MeV/c and an invariant mass $m_{\pi^+\gamma\gamma}$ between 400 and 1100 MeV/c^2.

For the $B^+ \to J/\psi\,K^+$ decay, the K^+ candidate is selected among particles that fulfil the same requirements applied to the charged pion in the $B^+ \to J/\psi\,\rho^+$ decay, have a transverse momentum larger than 800 MeV/c and are identified as a kaons.

The B^+ candidate is formed from the J/ψ candidate and the ρ^+ or K^+ candidate by requiring that the three recon-

[2] Throughout this publication, K^* refers to the $K^*(892)$ meson.

structed tracks form a good-quality vertex with significant displacement from the PV. In events with multiple PVs, that with which the B^+ candidate has the smallest $\chi^2_{\rm IP}$ is chosen. In addition, the B^+ candidate is constrained to originate from the PV using a kinematic fit [23]. In the $B^+ \to J/\psi\,\rho^+$ channel, the dimuon invariant mass is constrained to the known J/ψ mass, and when considering the invariant mass of the B^+ candidate, the π^0 candidate is additionally constrained to its known mass. This $\chi^2_{\rm IP}$ value is required to be small enough to be consistent with the B^+ meson having originated from the PV.

Decays of b hadrons with an additional charged particle are rejected by ensuring that the quality of the B^+ decay vertex significantly degrades when the closest additional track is included in the vertex fit. Finally, the mass of the B^+ candidate, $m_{J/\psi\,\pi^+\pi^0}$ ($m_{\mu^+\mu^-K^+}$), is required to be between 5100 and 5700 MeV/c^2 (5180 MeV/c^2 and 5400 MeV/c^2). For the $B^+ \to J/\psi\,K^+$ channel, this selection results in a good signal purity, and no further selection criteria are needed.

Two vetoes are applied for the $B^+ \to J/\psi\,\rho^+$ channel to reject $B^+ \to J/\psi\,K^+$ and $B^+ \to J/\psi\,\pi^+$ decays combined with a random π^0: the mass of the combination of the J/ψ and the charged pion candidate, evaluated under both the pion and kaon mass hypotheses, must be outside a 50 MeV/c^2 window around the known B^+ mass.

In addition to the preselection discussed above, a multivariate selection is performed on the $B^+ \to J/\psi\,\rho^+$ channel using an artificial neural network from the TMVA package [24,25], mainly to reduce combinatorial background. The 12 input variables are as follows: the flight distance and direction angle of the B^+ candidate, defined as the angle between its momentum and the vector connecting its primary and decay vertices; the transverse momentum of the B^+ and ρ^+ candidates; the maximum transverse momentum of the two muons, the $\chi^2_{\rm IP}$ of the charged pion; the minimum $\chi^2_{\rm IP}$ of the two muons; the quality of the B^+ candidate vertex; the change in the vertex quality when adding the closest track that is not part of the signal candidate; the quality of a kinematic fit of the full decay chain; the quality of the π^0 identification; and the $p_{\rm T}$ asymmetry in a cone around the flight direction of the B^+ meson, defined as $(\sum_i p_{{\rm T}i} - \sum_j p_{{\rm T}j})/(\sum_i p_{{\rm T}i} + \sum_j p_{{\rm T}j})$, where i runs over all final state tracks of $B^+ \to J/\psi\,\rho^+$ and j over all other tracks in a cone around the B^+ meson flight direction. The classifier is trained using background events from both a lower (4800–5000 MeV/c^2) and upper (5700–6000 MeV/c^2) sideband of the B^+ candidate mass and simulated signal decays, where the $p_{\rm T}$ distribution of the B^+ meson and the number of tracks per event are weighted to match the corresponding distributions in a $B^0 \to J/\psi\,K^{*0}$ data sample, where $K^{*0} \to K^+\pi^-$. The $B^0 \to J/\psi\,K^{*0}$ candidates are obtained using the same preselection on the charged particles as for the $B^+ \to J/\psi\,\rho^+$ decay, except that a looser particle-identification criterion is used for the pion. Moderate criteria are placed on the kaon p, $p_{\rm T}$ and particle identification to obtain a good signal purity. For quantities depending on the kinematics of the π^0 meson, the channel $B^+ \to J/\psi\,K^{*+}$, with $K^{*+} \to K^+\pi^0$, is used to compare the distributions of the input variables between simulation and data. For all variables good agreement is found.

The neural network selection criterion is optimized by maximizing the figure of merit $N_{\rm sig}/\sqrt{N_{\rm sig}+N_{\rm bg}}$, where $N_{\rm sig}$ is the expected number of signal decays and $N_{\rm bg}$ is the estimated background yield, both between 5200 MeV/c^2 and 5450 MeV/c^2. The value of $N_{\rm sig}$ is calculated using the ratio of the previously measured $B^+ \to J/\psi\,\rho^+$ and $B^+ \to J/\psi\,K^+$ branching fractions [14], the observed number of $B^+ \to J/\psi\,K^+$ decays, and the efficiencies of the $B^+ \to J/\psi\,\rho^+$ and $B^+ \to J/\psi\,K^+$ channels. The value of $N_{\rm bg}$ is obtained by extrapolating the shape of the background into the signal region. The optimized cut rejects 99.4% of background events in both, the 2011 and 2012 data samples, while retaining 49% (45%) of signal events in the 2011 (2012) data samples.

After applying the full selection for $B^+ \to J/\psi\,\rho^+$ decays, about 9% of events have more than one candidate. Most of these events contain a genuine $B^+ \to J/\psi\,\rho^+$ decay, along with a candidate comprised of the charged particles from the signal decay combined with a prompt π^0 meson. The latter constitutes a peaking background that is difficult to model, and therefore, events with multiple candidates are removed from the analysis. The efficiency of this rejection is evaluated on simulated samples. The sample of $B^+ \to J/\psi\,K^+$ decays contains only 0.2% events with multiple candidates and no rejection is required.

4 Efficiencies

The branching ratio of the decay $B^+ \to J/\psi\,\rho^+$ is calculated using

$$\mathcal{B}(B^+ \to J/\psi\,\rho^+) = \mathcal{B}(B^+ \to J/\psi\,K^+) \times \frac{N_{B^+\to J/\psi\,\rho^+}}{N_{B^+\to J/\psi\,K^+}} \times \frac{\varepsilon_{B^+\to J/\psi\,K^+}}{\varepsilon_{B^+\to J/\psi\,\rho^+}} \times \frac{1}{\mathcal{B}(\pi^0 \to \gamma\gamma)}, \quad (2)$$

with $N_{B^+\to J/\psi\,\rho^+}$ ($N_{B^+\to J/\psi\,K^+}$) the number of measured $B^+ \to J/\psi\,\rho^+$ ($B^+ \to J/\psi\,K^+$) decays and $\varepsilon_{B^+\to J/\psi\,\rho^+}$ ($\varepsilon_{B^+\to J/\psi\,K^+}$) the efficiency for the $B^+ \to J/\psi\,\rho^+$ ($B^+ \to J/\psi\,K^+$) channel. The efficiencies $\varepsilon_{B^+\to J/\psi\,K^+}$ and $\varepsilon_{B^+\to J/\psi\,\rho^+}$ are composed of the geometrical acceptance, trigger, reconstruction, particle identification and selection efficiencies. In addition, there is an efficiency due to the removal of multiple candidates in the $B^+ \to J/\psi\,\rho^+$ sample. The efficiency for the decay products of a $B^+ \to J/\psi\,\rho^+$

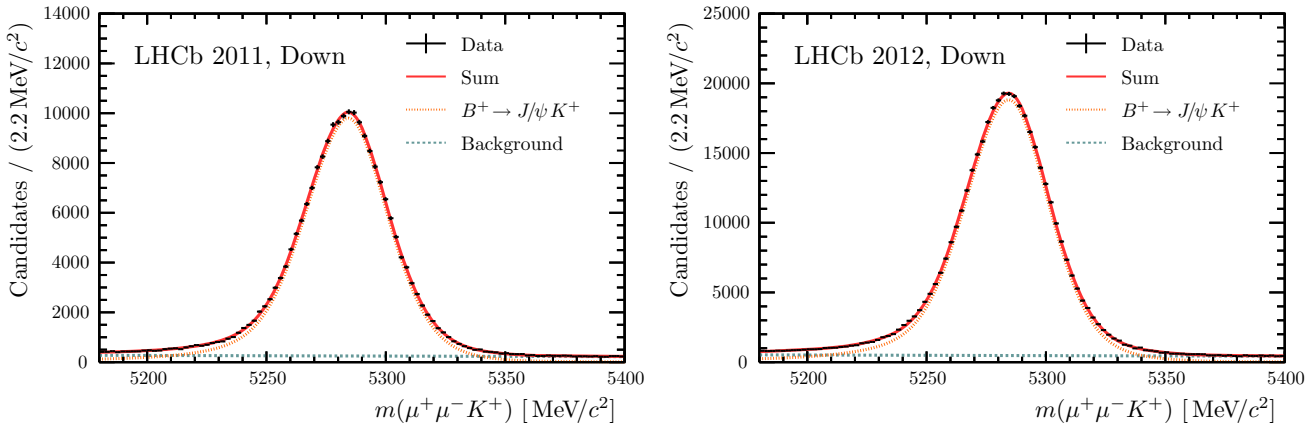

Fig. 2 The $\mu^+\mu^-K^+$ invariant mass distributions for the (left) 2011 and (right) 2012 data sets with down magnet polarity

or $B^+ \to J/\psi\, K^+$ decay to be within the acceptance of the LHCb detector is taken from simulation. The efficiency to trigger on one or both muons from the J/ψ decay is also taken from simulation. When forming the ratio of branching fractions between the $B^+ \to J/\psi\, \rho^+$ and $B^+ \to J/\psi\, K^+$ decays, the ratio of trigger efficiencies is close to unity.

The charged-particle reconstruction efficiency is taken from simulation with kinematics-dependent correction factors applied that are determined using a tag-and-probe technique applied on a detached $J/\psi \to \mu^+\mu^-$ data sample [26]. The π^0 reconstruction efficiency is also obtained from simulation, with a p_{T}-dependent correction factor obtained from the deviation between the known and observed ratio of branching fractions of $B^+ \to J/\psi\, K^+$ and $B^+ \to J/\psi\, K^{*+}$ decays, with $K^{*+} \to K^+\pi^0$ followed by $\pi^0 \to \gamma\gamma$ [27]. Data samples of $B^+ \to J/\psi\, K^+$ and $B^+ \to J/\psi\, K^{*+}$ decays, collected in 2011 and 2012 by the LHCb experiment, are fitted to obtain the number of observed decays. After correcting for the charged-particle selection efficiencies, the double ratio between the ratio of observed decays and the ratio of known branching fractions is the efficiency to reconstruct a π^0 meson. This result is compared to the π^0 efficiency obtained from simulated samples to determine the correction factors in intervals of the p_{T} of the π^0 meson. Using this procedure, the uncertainty on the branching fraction of the $B^+ \to J/\psi\, K^+$ decay cancels in the measurement of the $B^+ \to J/\psi\, \rho^+$ branching fraction, and only the uncertainty on the branching fraction of the $B^+ \to J/\psi\, K^{*+}$ decay contributes.

The charged-particle identification efficiency is evaluated using a tag-and-probe technique on dedicated calibration data samples with clean signatures [28]. Given the similar kinematics for the muons from $B^+ \to J/\psi\, \rho^+$ and $B^+ \to J/\psi\, K^+$ decays, the muon identification efficiency fully cancels when forming the ratio of branching fractions. The charged-pion identification efficiency is 72% for the 2011 data and 74% for the 2012 data. The efficiencies for identifying positively and negatively charged pions are compatible within their statistical uncertainties. The efficiency for identifying the kaon is above 95% for both data taking periods.

The remaining offline selection efficiencies are taken from simulation, where all kinematic distributions for the signal decay are found to be compatible with the corresponding distributions observed in data for $B^0 \to J/\psi\, K^{*0}$ and $B^+ \to J/\psi\, K^{*+}$ decays.

5 Invariant mass fits

The yield of $B^+ \to J/\psi\, K^+$ decays is determined using an extended unbinned maximum-likelihood fit to the $m_{\mu^+\mu^-K^+}$ distribution. The signal shape is described using the sum of two Crystal Ball functions [29] and a Gaussian function, where all three functions share the peak position value. The tail parameters of the Crystal Ball functions are fixed to the values obtained from simulation. An exponential function is used to model the combinatorial background. The fit yields a total of $362\,739 \pm 992$ $B^+ \to J/\psi\, K^+$ decays in 2011 and $816\,197 \pm 1545$ in 2012. The fit is performed separately for the two magnet polarities; Figure 2 shows the fit to the data taken with down polarity.

The yield of $B^+ \to J/\psi\, \rho^+$ decays is determined using a simultaneous two-dimensional extended unbinned maximum-likelihood fit to the $m_{J/\psi\,\pi^+\pi^0}$ and $m_{\pi^+\gamma\gamma}$ distributions in the 2011 and 2012 data sets. The signal shape in $m_{J/\psi\,\pi^+\pi^0}$ is modelled with the sum of two Crystal Ball functions with a shared peak position value. The values of the tail parameters are taken from simulation. The signal shape in $m_{\pi^+\gamma\gamma}$ is modelled with a relativistic Breit–Wigner function

$$\mathcal{P}_{\rho^+}(m_{\pi^+\gamma\gamma}) = \frac{m_{\pi^+\gamma\gamma}\,\Gamma(m_{\pi^+\gamma\gamma})\,P_{J/\psi}^{2L_{\mathrm{eff}}+1}}{(m_{\rho^+}^2 - m_{\pi^+\gamma\gamma}^2)^2 + m_{\rho^+}^2\,\Gamma(m_{\pi^+\gamma\gamma})^2}, \quad (3)$$

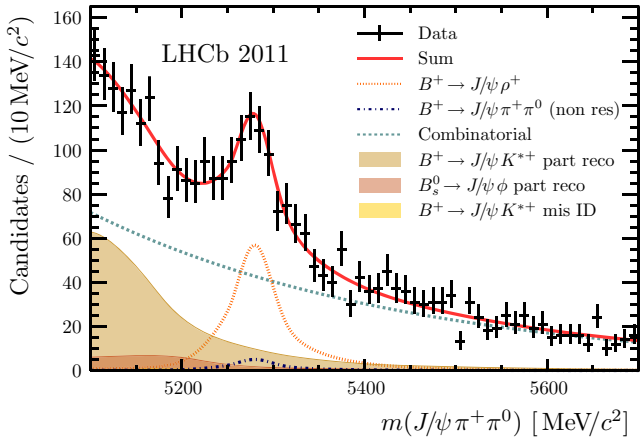

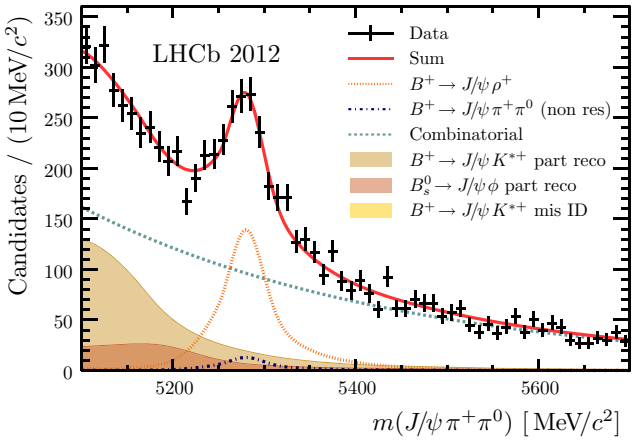

Fig. 3 The $J/\psi\pi^+\pi^0$ invariant mass distributions for the (left) 2011 and (right) 2012 data sets. In the legend, "non res" stands for non-resonant background, "part reco" for partially reconstructed background and "mis ID" for background involving a misidentification of a kaon. The mis ID background is small and not visible in these figures

with

$$\Gamma(m_{\pi^+\gamma\gamma}) = \Gamma_0 \left(\frac{q}{q_0}\right)^3 \left(\frac{m_{\rho^+}}{m_{\pi^+\gamma\gamma}}\right) \left(\frac{1+R^2q_0^2}{1+R^2q^2}\right). \quad (4)$$

Here, $P_{J/\psi}$ is the momentum of the J/ψ meson in the B^+ rest frame, $q(m_{\pi^+\gamma\gamma})$ is the pion momentum in the dipion rest frame, L_{eff} is the relative angular momentum of the ρ^+ meson with respect to the J/ψ, $q_0 = q(m_{\rho^+})$, Γ_0 is the nominal width, and R is a barrier factor radius. The tail parameters of the Crystal Ball function, along with m_{ρ^+} and Γ_0 of the Breit–Wigner, are fixed to values obtained from a fit to simulated $B^+ \to J/\psi\,\rho^+$ decays, generated using the same functional form with input values $m_{\rho^+} = 768.5\,\text{MeV/c}^2$ and $\Gamma_0 = 151\,\text{MeV/c}^2$. This strategy therefore folds in the effect of the $m_{\pi^+\gamma\gamma}$ resolution into the Breit–Wigner model, which results in a value of $\Gamma_0 = 175\,\text{MeV/c}^2$. The relative angular momentum L_{eff} is fixed to 0.

Non-resonant $J/\psi\pi^+\pi^0$ decays are described with the same shape as the signal in $m_{J/\psi\pi^+\pi^0}$, while in $m_{\pi^+\gamma\gamma}$ a three-body phase-space distribution multiplied by $P^2_{J/\psi}$ is used, which is motivated by angular momentum conservation. Given the slowly varying shape in $m_{\pi^+\gamma\gamma}$, no description of the detector resolution is needed. The combinatorial background is described by an exponential function in $m_{J/\psi\pi^+\pi^0}$ and a first-order polynomial in $m_{\pi^+\gamma\gamma}$.

Two partially reconstructed backgrounds are included in the $B^+ \to J/\psi\,\rho^+$ fit. The first is the decay $B^+ \to J/\psi\,K^{*+}$, with $K^{*+} \to K^0_S\pi^+$ and $K^0_S \to \pi^0\pi^0$, where one π^0 is not reconstructed. The second is the decay $B^0_s \to J/\psi\,\phi$, with $\phi \to \pi^+\pi^-\pi^0$, where one charged pion is not reconstructed. As the shapes of both contributions exhibit significant correlations between $m_{J/\psi\pi^+\pi^0}$ and $m_{\pi^+\gamma\gamma}$, they are described by two-dimensional kernel density estimators [30] with adaptive kernels determined using simulation.

The final component is the background from $B^+ \to J/\psi\,K^{*+}$ decays, with $K^{*+} \to K^+\pi^0$, where the kaon is misidentified as a pion. Despite the stringent particle-identification criterion applied, a small amount of these decays is present in the final sample. The product of two one-dimensional kernel density estimators is used to describe the shape in the two invariant mass distributions. This background yield is fixed relative to that of the $B^+ \to J/\psi\,K^{*+}$ decay, with $K^{*+} \to K^0_S\pi^+$, using the known ratio of the branching fractions [14].

The one-dimensional projections of the two-dimensional simultaneous fit to the 2011 and 2012 data set are shown in Fig. 3 for $m_{J/\psi\pi^+\pi^0}$ and in Fig. 4 for $m_{\pi^+\gamma\gamma}$, where only events between 5250 and 5310 MeV/c^2 in $m_{J/\psi\pi^+\pi^0}$ are considered. For the full fit regions in $m_{J/\psi\pi^+\pi^0}$ and $m_{\pi^+\gamma\gamma}$ a total of 489 ± 32 (1090 ± 70) signal decays are observed in 2011 (2012). The fraction of $B^+ \to J/\psi\,\pi^+\pi^0$ decays that do not proceed via the ρ^+ resonance is measured to be $(8.4^{+6.1}_{-6.2})\%$ in the $m_{\pi^+\gamma\gamma}$ interval from 400 MeV/c^2 to 1100 MeV/c^2.

The value of $\mathcal{A}^{CP}$ is calculated using

$$\mathcal{A}^{CP} = \mathcal{A}^{CP}_{\text{raw}} - \mathcal{A}^{\text{prod}}, \quad (5)$$

where $\mathcal{A}^{CP}_{\text{raw}}$ is the raw asymmetry, determined from a fit to the 2011 and 2012 data sets, split by the charge of the B meson, where all fit components are modelled as in the branching fraction measurement; and $\mathcal{A}^{\text{prod}}$ is the production asymmetry of B^+ mesons in LHCb. For 2011 and 2012 they were measured to be $(-0.41 \pm 0.49 \pm 0.11)\%$ and $(-0.53 \pm 0.31 \pm 0.10)\%$, respectively [31], with the first uncertainty being statistical and the second systematic.

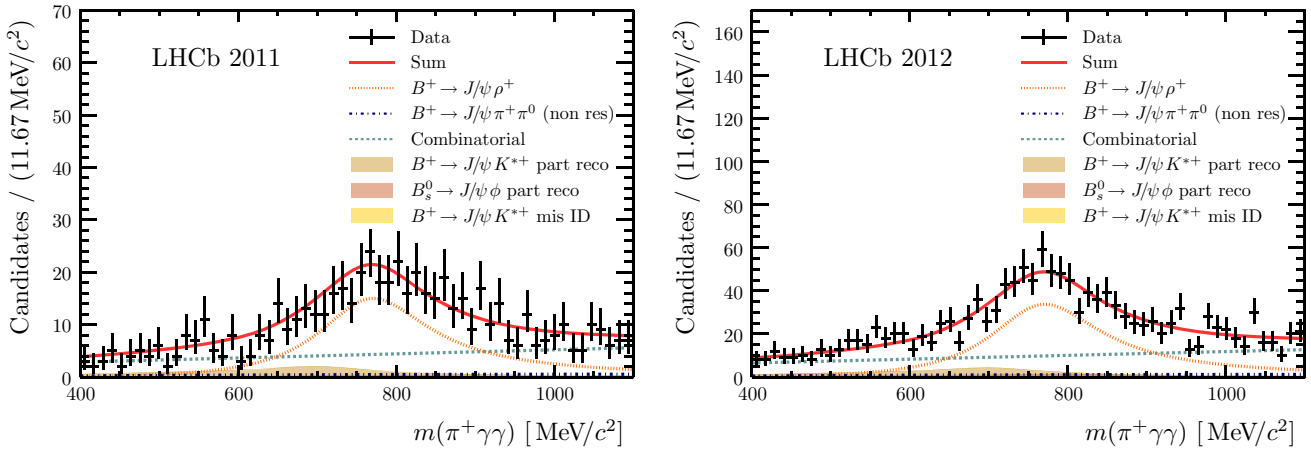

Fig. 4 The $\pi^+\gamma\gamma$ invariant mass distributions for the (left) 2011 and (right) 2012 data sets for $m_{J/\psi\pi^+\pi^0}$ between 5250 and 5310 MeV/c^2. The part reco and mis ID backgrounds are small in the given mass region and not visible in these figures

For the background contribution from the $B^+ \to J/\psi\, K^{*+}$ decay with $K^{*+} \to K^0_S\pi^+$, the CP asymmetry is fixed to the known value of $(-4.8 \pm 3.3)\%$ [14] after correcting for the production asymmetry. For the partially reconstructed background from $B^0_s \to J/\psi\,\phi$ decays, no charge asymmetry is expected, as the final state is identical for both B^0_s and $\overline{B}{}^0_s$ mesons.

6 Systematic uncertainties

6.1 Uncertainties on the branching fraction

The systematic uncertainties for the branching fraction measurement are summarized in Table 1. The trigger efficiencies are derived from simulation. The ratio of efficiencies for $B^+ \to J/\psi\, K^+$ and $B^+ \to J/\psi\,\rho^+$ decays has a small deviation from unity due to the slightly different kinematical distributions of the J/ψ mesons. To account for potential mismodelling of the impact of the K^+ and ρ^+ on the J/ψ trigger efficiency in simulation, the p_{T} distributions of the B^+ and J/ψ mesons in $B^+ \to J/\psi\, K^+$ decays are weighted to match those in $B^+ \to J/\psi\,\rho^+$ decays, and the trigger efficiency is reevaluated. The resulting difference between this ratio of trigger efficiencies and unity is taken as a systematic uncertainty.

For the charged-particle reconstruction efficiency, the correction factors between simulation and data are varied within their uncertainties, and the effect on the ratio of $B^+ \to J/\psi\,\rho^+$ and $B^+ \to J/\psi\, K^+$ decays is evaluated. The uncertainties consist of both statistical and systematic components, where the latter are due to the limited precision on the knowledge of the LHCb material budget. Only the contribution of the material budget uncertainty and the different interaction cross-section of pions and kaons with the material significantly contribute to the uncertainty.

Table 1 Systematic uncertainties on the branching fraction $\mathcal{B}(B^+ \to J/\psi\,\rho^+)$

Source of uncertainty	Relative uncertainty [%]
Trigger efficiency	1.4
Charged particle reconstruction efficiency	0.5
π^0 reconstruction efficiency	6.3
Hadron identification efficiency	2.1
Muon identification efficiency	0.4
Selection efficiency $B^+ \to J/\psi\, K^+$	0.1
Selection efficiency $B^+ \to J/\psi\,\rho^+$	1.8
Removal of multiple candidates	1.2
Fit function	4.0
$B^+ \to J/\psi\,\rho^+$ polarization	2.2
Fit ranges	1.6
Nonresonant line shape	1.5
Neglecting interference	2.8
Quadratic sum	9.1

The uncertainty on the π^0 reconstruction efficiency is dominated by the uncertainty on the branching fraction of the $B^+ \to J/\psi\, K^{*+}$ decay, which is used in its calculation, and the number of $B^+ \to J/\psi\, K^{*+}$ candidates in each kinematic bin. These values are added in quadrature to the systematic uncertainty of the method.

The systematic uncertainty for the charged-pion identification efficiency is evaluated by calculating the difference in efficiency between the nominal method, which is performed in intervals of p_{T}, pseudorapidity, and the number of tracks in the event, and an alternative, unbinned method. In addition,

a different quantity for the event multiplicity and a different scheme of interval boundaries are used. All three uncertainties are added in quadrature. A similar procedure is used for the kaon and muon identification efficiencies, resulting in smaller systematic uncertainties.

For $B^+ \to J/\psi K^+$ decays, the uncertainty on the selection efficiency is dominated by the limited size of the simulated data set. For the $B^+ \to J/\psi \rho^+$ selection, the largest component of this uncertainty arises from potential discrepancies in the π^0 identification variable between simulation and data. The decay $B^+ \to J/\psi K^{*+}$ is used to weight the distribution of this variable, and the change in the multivariate classifier efficiency with respect to the baseline value is taken as a systematic uncertainty. A smaller contribution comes from the limited size of the simulated data set.

The uncertainty on the procedure to remove multiple-candidate events in the $B^+ \to J/\psi \rho^+$ channel is determined on simulation by calculating the efficiency to select events that contain only one candidate, where the simulated events are weighted so that the event occupancy matches that observed in data. In addition, the invariant mass distributions in data are fitted for all events and events that only contain one candidate, where the signal shape is unchanged for both fits, *i.e.* the peaking background arising when the charged particles from a genuine signal decay are combined with a prompt π^0 meson is ignored. The difference in efficiency between data and simulation is taken as a systematic uncertainty.

The two-dimensional kernel density estimators use adaptive kernel widths. The effect of the kernel width is tested by setting it to a constant value, either higher or lower than the default value, and taking the resulting difference in the branching fraction as a systematic uncertainty. The tail parameters of the Crystal Ball function in $B^+ \to J/\psi \rho^+$ decays are varied by $\pm 20\%$ with respect to the baseline values to account for the uncertainties in the fit to simulation. The value of m_{ρ^+} of the Breit–Wigner function is left free to vary, instead of being fixed to its baseline value. Furthermore, to take a possible difference in the experimental resolution of the ρ^+ mass between data and simulation into account, the value of Γ_0 of the Breit–Wigner shape is altered by the difference in the width of the B^+ mass peak between data and simulation in the decay $B^+ \to J/\psi K^{*+}$. All differences with respect to the branching fraction of the baseline fit are added in quadrature and added to the overall systematic uncertainty. To take possible correlations in the signal shape between $m_{J/\psi \pi^+\pi^0}$ and $m_{\pi^+\gamma\gamma}$ into account, the baseline model is replaced by a two-dimensional kernel density estimator whose shape is obtained from simulation. The resulting difference in the branching fraction with respect to the baseline model is taken as a systematic uncertainty.

The polarization of the decay products of the B^+ meson in the $B^+ \to J/\psi \rho^+$ decay is unknown. Using simulated decays where L_{eff} is set to 1 or 2, the branching fraction is recalculated and the difference in the observed branching fraction with respect to the baseline result is taken as a systematic uncertainty. As a consistency test, simulated decays with $L_{\text{eff}} = 0$ are studied. A small bias with respect to the baseline branching fraction is observed, which is corrected for and taken as a systematic uncertainty.

To test the effect of different polarization amplitudes of $B^+ \to J/\psi \rho^+$ in simulation and data on the efficiency to reconstruct the decay, the values of the helicity amplitudes from $B^0 \to J/\psi \rho^0$ [32] are used in the simulation of $B^+ \to J/\psi \rho^+$ decays and varied within their uncertainties. The largest deviation with respect to the baseline value is taken as a systematic uncertainty.

In order to estimate the systematic uncertainty from the chosen fit range, the fit to determine the branching fraction is repeated 1000 times with random intervals in $m_{J/\psi \pi^+\pi^0}$ and $m_{\pi^+\gamma\gamma}$ larger or smaller than those of the baseline fit. The width of the resulting distribution of the measured branching fractions of $B^+ \to J/\psi \rho^+$ decays for each interval is taken as a systematic uncertainty. A small bias with respect to the baseline result was observed. The bias is corrected for and also taken as a systematic uncertainty.

As an alternative modelling for the nonresonant contribution in $m_{\pi^+\gamma\gamma}$, the shape is modelled with the form $(P_{J/\psi}/m_B)^2$ [33], with m_B the known mass of the B^+ meson [14]. The difference of the branching fraction with respect to the baseline fit is taken as a systematic uncertainty.

A contribution from interference between the nonresonant $B^+ \to J/\psi \pi^+\pi^0$ and signal $B^+ \to J/\psi \rho^+$ decays could arise due to an asymmetric efficiency of the angular distribution of the $\pi^+\pi^0$ system. To assess the effect of not taking the interference term in the branching fraction fit into account, several samples of one million simulated decays are generated including the interference term, where for each sample a different fixed phase for the nonresonant contribution is chosen. The shape of the angular acceptance is taken from the full simulation of $B^+ \to J/\psi \rho^+$ decays. Each sample is fitted with the baseline description, which does not include the interference term. The largest relative difference in the signal yield with respect to the generated value is taken as a systematic uncertainty. To investigate possible exotic resonance contributions, the invariant masses of $J/\psi \pi^+$ and $J/\psi \pi^0$ are inspected and no excess compared to the expectation is found.

Given the nature of the systematic uncertainties on the π^0 and charged-particle reconstruction efficiencies, the selection efficiency and the removal of multiple candidates, their correlation in 2011 and 2012 is set to 1. All other uncertainties either result from a common fit to the combined data sets of 2011 and 2012 or are treated as uncorrelated.

Table 2 Systematic uncertainties on the direct CP asymmetry of $B^+ \to J/\psi\,\rho^+$ decays

Source of uncertainty	Uncertainty
B^+ production asymmetry and background asymmetry	0.006
Signal fit function	0.005
Pion detection asymmetry	0.003
Quadratic sum	0.008

6.2 Uncertainties on the CP asymmetry

Most systematic uncertainties cancel when calculating the $\mathcal{A}^{CP}$ ratio. The remaining contributions are listed in Table 2. The largest contributions come from the uncertainty on the knowledge of the direct CP asymmetry of the $B^+ \to J/\psi\,K^{*+}$ decay for the partially reconstructed background, and the limited knowledge of the production asymmetry for B^+ mesons in the 2011 and 2012 data sets. The signal model is again replaced by a two-dimensional kernel density estimator to take possible correlations into account, taking the difference in the CP-asymmetry results as a systematic uncertainty. The ratio of the positive and negative pion detection efficiencies $\varepsilon(\pi^+)/\varepsilon(\pi^-)$ has been measured at the LHCb experiment [12] and found to be compatible with unity over a broad range of momenta and transverse momenta, with an uncertainty of about 0.5%. This uncertainty is added as a systematic uncertainty for $\mathcal{A}^{CP}$.

To evaluate a possible bias on the asymmetry result, a permutation test is performed where the data set is split 1000 times randomly, instead of by the charge of the B^+ meson, and the asymmetry is evaluated. As an additional check, simulated decays are added to each of these randomly split samples, corresponding to $\pm 5\%$ and $\pm 10\%$ asymmetry, to assess the robustness of the asymmetry fit for a non-zero $\mathcal{A}^{CP}$ value. No bias in the resulting distributions is observed. The total systematic uncertainty for $\mathcal{A}^{CP}$ is formed by adding all individual components in quadrature.

7 Results and summary

Using Eq. (2) the ratio of the branching fractions of the decays $B^+ \to J/\psi\,\rho^+$ and $B^+ \to J/\psi\,K^+$ is determined to be

$$\frac{\mathcal{B}(B^+ \to J/\psi\,\rho^+)}{\mathcal{B}(B^+ \to J/\psi\,K^+)} = 0.0378^{+0.0025}_{-0.0024} \pm 0.0035$$

in a combined fit to the 2011 and 2012 data sets, where the first uncertainty is statistical and the second systematic. The ratio of efficiencies $\frac{\varepsilon_{B^+ \to J/\psi\,K^+}}{\varepsilon_{B^+ \to J/\psi\,\rho^+}}$ is 27.2 ± 2.0 for the combination of both data sets, it is dominated by the low efficiency to select a π^0 with a sufficiently high transverse momentum.

The branching fraction for the decay $B^+ \to J/\psi\,\rho^+$ is

$$\mathcal{B}(B^+ \to J/\psi\,\rho^+) = (3.81^{+0.25}_{-0.24} \pm 0.35) \times 10^{-5}.$$

The CP asymmetry is measured to be

$$\mathcal{A}^{CP}(B^+ \to J/\psi\,\rho^+) = -0.045^{+0.056}_{-0.057} \pm 0.008.$$

Both results are the most precise to date and are consistent with previous measurements. Furthermore, the measured value of $\mathcal{A}^{CP}$ is consistent with the corresponding measurement using $B^0 \to J/\psi\,\rho^0$ decays, as expected from isospin symmetry [2].

Acknowledgements We express our gratitude to our colleagues in the CERN accelerator departments for the excellent performance of the LHC. We thank the technical and administrative staff at the LHCb institutes. We acknowledge support from CERN and from the national agencies: CAPES, CNPq, FAPERJ and FINEP (Brazil); MOST and NSFC (China); CNRS/IN2P3 (France); BMBF, DFG and MPG (Germany); INFN (Italy); NWO (Netherlands); MNiSW and NCN (Poland); MEN/IFA (Romania); MSHE (Russia); MinECo (Spain); SNSF and SER (Switzerland); NASU (Ukraine); STFC (United Kingdom); NSF (USA). We acknowledge the computing resources that are provided by CERN, IN2P3 (France), KIT and DESY (Germany), INFN (Italy), SURF (Netherlands), PIC (Spain), GridPP (United Kingdom), RRCKI and Yandex LLC (Russia), CSCS (Switzerland), IFIN-HH (Romania), CBPF (Brazil), PL-GRID (Poland) and OSC (USA). We are indebted to the communities behind the multiple open-source software packages on which we depend. Individual groups or members have received support from AvH Foundation (Germany); EPLANET, Marie Skłodowska-Curie Actions and ERC (European Union); ANR, Labex P2IO and OCEVU, and Région Auvergne-Rhône-Alpes (France); Key Research Program of Frontier Sciences of CAS, CAS PIFI, and the Thousand Talents Program (China); RFBR, RSF and Yandex LLC (Russia); GVA, XuntaGal and GENCAT (Spain); the Royal Society and the Leverhulme Trust (United Kingdom); Laboratory Directed Research and Development program of LANL (USA).

Data Availability Statement This manuscript has no associated data or the data will not be deposited. [Author's comment: All LHCb scientific output is published in journals, with preliminary results made available in Conference Reports. All are Open Access, without restriction on use beyond the standard conditions agreed by CERN. Data associated to the plots in this publication as well as in supplementary materials are made available on the CERN document server at http://cdsweb.cern.ch/record/2652406. This information is taken from the LHCb External Data Access Policy which can be downloaded at http://opendata.cern.ch/record/410.]

Funded by SCOAP[3].

References

1. P. Frings, U. Nierste, M. Wiebusch, Penguin contributions to CP phases in $B_{d,s}$ decays to charmonium. Phys. Rev. Lett. **115**, 061802 (2015). arxiv:1503.00859

2. LHCb collaboration, R. Aaij et al., Measurement of the CP-violating phase β in $\overline{B}^0 \to J/\psi\pi^+\pi^-$ decays and limits on penguin effects, Phys. Lett. B **742**, 38, (2015). arXiv:1411.1634
3. S. Faller, R. Fleischer, T. Mannel, Precision physics with $B_s^0 \to J/\psi\phi$ at the LHC: The quest for new physics. Phys. Rev. D **79**, 014005 (2009). arXiv:0810.4248
4. R. Fleischer, Extracting CKM phases from angular distributions of $B_{d,s}$ decays into admixtures of CP eigenstates. Phys. Rev. D **60**, 073008 (1999). arXiv:9903540
5. BaBar collaboration, B. Aubert et al., Branching fraction and charge asymmetry measurements in $B \to J/\psi\pi\pi$ decays, Phys. Rev. D **76**, 031101, (2007) arXiv:0704.1266
6. LHCb collaboration, A. A. Alves Jr. et al., The LHCb detector at the LHC. JINST **3**, S08005 (2008)
7. LHCb collaboration, R. Aaij et al., LHCb detector performance. Int. J. Mod. Phys. A **30**, 1530022 (2015). arXiv:1412.6352
8. R. Aaij et al., Performance of the LHCb Vertex Locator. JINST **9**, P09007 (2014). arXiv:1405.7808
9. R. Arink et al., Performance of the LHCb outer tracker. JINST **9**, P01002 (2014). arXiv:1311.3893
10. M. Adinolfi et al., Performance of the LHCb RICH detector at the LHC. Eur. Phys. J. C **73**, 2431 (2013). arXiv:1211.6759
11. A.A. Alves Jr. et al., Performance of the LHCb muon system. JINST **8**, P02022 (2013). arXiv:1211.1346
12. LHCb collaboration, R. Aaij et al., Measurement of the $D_s^+ - D_s^-$ production asymmetry in 7 Tev pp collisions. Phys. Lett. B **713**, 186 (2012). arXiv:1205.0897
13. R. Aaij et al., The LHCb trigger and its performance in 2011. JINST **8**, P04022 (2013). arXiv:1211.3055
14. Particle Data Group, M. Tanabashi et al., Review of particle physics. Phys. Rev. D **98**, 030001 (2018)
15. T. Sjöstrand, S. Mrenna, P. Skands, PYTHIA 6.4 physics and manual. JHEP **05**, 026 (2006). arXiv:hep-ph/0603175
16. T. Sjöstrand, S. Mrenna, P. Skands, A brief introduction to PYTHIA 8.1. Comput. Phys. Commun. **178**, 852 (2008). arXiv:0710.3820
17. I. Belyaev et al., Handling of the generation of primary events in Gauss, the LHCb simulation framework. J. Phys. Conf. Ser. **331**, 032047 (2011)
18. D.J. Lange, The EvtGen particle decay simulation package. Nucl. Instrum. Methods A **462**, 152 (2001)
19. P. Golonka, Z. Was, PHOTOS Monte Carlo: a precision tool for QED corrections in Z and W decays. Eur. Phys. J. C **45**, 97 (2006). arXiv:hep-ph/0506026
20. Geant4 collaboration, J. Allison et al., Geant4 developments and applications. IEEE Trans. Nucl. Sci. **53**, 270 (2006)
21. Geant4 collaboration, S. Agostinelli *et al.*, Geant4: A simulation toolkit. Nucl. Instrum. Methods A **506**, 250 (2003)
22. M. Clemencic et al., The LHCb simulation application, Gauss: Design, evolution and experience. J. Phys. Conf. Ser. **331**, 032023 (2011)
23. W.D. Hulsbergen, Decay chain fitting with a Kalman filter. Nucl. Instrum. Methods A **552**, 566 (2005). arXiv:physics/0503191
24. H. Voss, A. Hoecker, J. Stelzer, F. Tegenfeldt, TMVA-toolkit for multivariate data analysis. PoS **ACAT**, 040 (2007)
25. A. Hoecker et al., TMVA 4—toolkit for multivariate data analysis. Users Guide. arXiv:physics/0703039
26. LHCb collaboration, R. Aaij, et al., Measurement of the track reconstruction efficiency at LHCb, JINST **10**, P02007 (2015). arXiv:1408.1251
27. LHCb collaboration, R. Aaij et al., Evidence for the decay $B^0 \to J/\psi\omega$ and measurement of the relative branching fractions of B_s^0 meson decays to $J/\psi\eta$ and $J/\psi\eta'$, Nucl. Phys. B **867**, 547 (2013). arXiv:1210.2631
28. L. Anderlini et al. The PIDCalib package, LHCb-PUB-2016-021
29. T. Skwarnicki, A study of the radiative cascade transitions between the Upsilon-prime and Upsilon resonances, PhD thesis, Institute of Nuclear Physics, Krakow (1986), DESY-F31-86-02
30. K.S. Cranmer, Kernel estimation in high-energy physics. Comput. Phys. Commun. **136**, 198 (2001). arXiv:hep-ex/0011057
31. LHCb collaboration, R. Aaij et al., Measurement of the $B^\pm$ production asymmetry and the CP asymmetry in $B^\pm \to J/\psi K^\pm$ decays. Phys. Rev. D **95**, 052005 (2017). arXiv:1701.05501
32. LHCb collaboration, R. Aaij et al., Measurement of the resonant and CP components in $\overline{B}^0 \to J/\psi\pi^+\pi^-$ decays. Phys. Rev. D **90**, 012003 (2014). arXiv:1404.5673
33. LHCb collaboration, R. Aaij et al., Analysis of the resonant components in $\overline{B}^0 J/\psi\pi^+\pi^-$. Phys. Rev. D **87**, 052001 (2013). arXiv:1301.5347

LHCb Collaboration

R. Aaij[28], C. Abellán Beteta[46], B. Adeva[43], M. Adinolfi[50], C. A. Aidala[77], Z. Ajaltouni[6], S. Akar[61], P. Albicocco[19], J. Albrecht[11], F. Alessio[44], M. Alexander[55], A. Alfonso Albero[42], G. Alkhazov[34], P. Alvarez Cartelle[57], A. A. Alves Jr[43], S. Amato[2], S. Amerio[24], Y. Amhis[8], L. An[3], L. Anderlini[18], G. Andreassi[45], M. Andreotti[17], J. E. Andrews[62], F. Archilli[28], P. d'Argent[13], J. Arnau Romeu[7], A. Artamonov[41], M. Artuso[63], K. Arzymatov[38], E. Aslanides[7], M. Atzeni[46], B. Audurier[23], S. Bachmann[13], J. J. Back[52], S. Baker[57], V. Balagura[8,b], W. Baldini[17], A. Baranov[38], R. J. Barlow[58], G. C. Barrand[8], S. Barsuk[8], W. Barter[58], M. Bartolini[20], F. Baryshnikov[74], V. Batozskaya[32], B. Batsukh[63], A. Battig[11], V. Battista[45], A. Bay[45], J. Beddow[55], F. Bedeschi[25], I. Bediaga[1], A. Beiter[63], L. J. Bel[28], S. Belin[23], N. Beliy[66], V. Bellee[45], N. Belloli[21,i], K. Belous[41], I. Belyaev[35], E. Ben-Haim[9], G. Bencivenni[19], S. Benson[28], S. Beranek[10], A. Berezhnoy[36], R. Bernet[46], D. Berninghoff[13], E. Bertholet[9], A. Bertolin[24], C. Betancourt[46], F. Betti[16,44], M. O. Bettler[51], M. van Beuzekom[28], Ia. Bezshyiko[46], S. Bhasin[50], J. Bhom[30], S. Bifani[49], P. Billoir[9], A. Birnkraut[11], A. Bizzeti[18,u], M. Bjørn[59], M. P. Blago[44], T. Blake[52], F. Blanc[45], S. Blusk[63], D. Bobulska[55], V. Bocci[27], O. Boente Garcia[43], T. Boettcher[60], A. Bondar[40,x], N. Bondar[34], S. Borghi[44,58], M. Borisyak[38], M. Borsato[43], F. Bossu[8], M. Boubdir[10], T. J. V. Bowcock[56], C. Bozzi[17,44], S. Braun[13], M. Brodski[44], J. Brodzicka[30], A. Brossa Gonzalo[52], D. Brundu[23,44], E. Buchanan[50], A. Buonaura[46], C. Burr[58], A. Bursche[23], J. Buytaert[44], W. Byczynski[44], S. Cadeddu[23], H. Cai[68], R. Calabrese[17,g], R. Calladine[49], M. Calvi[21,i], M. Calvo Gomez[42,m], A. Camboni[42,m], P. Campana[19], D. H. Campora Perez[44], L. Capriotti[16], A. Carbone[16,e], G. Carboni[26], R. Cardinale[20], A. Cardini[23], P. Carniti[21,i], L. Carson[54], K. Carvalho Akiba[2], G. Casse[56], L. Cassina[21], M. Cattaneo[44],

G. Cavallero[20,h], R. Cenci[25,p], D. Chamont[8], M. G. Chapman[50], M. Charles[9], Ph. Charpentier[44], G. Chatzikonstantinidis[49], M. Chefdeville[5], V. Chekalina[38], C. Chen[3], S. Chen[23], S.-G. Chitic[44], V. Chobanova[43], M. Chrzaszcz[44], A. Chubykin[34], P. Ciambrone[19], X. Cid Vidal[43], G. Ciezarek[44], P. E. L. Clarke[54], M. Clemencic[44], H. V. Cliff[51], J. Closier[44], V. Coco[44], J. A. B. Coelho[8], J. Cogan[7], E. Cogneras[6], L. Cojocariu[33], P. Collins[44], T. Colombo[44], A. Comerma-Montells[13], A. Contu[23], G. Coombs[44], S. Coquereau[42], G. Corti[44], M. Corvo[17,g], C. M. Costa Sobral[52], B. Couturier[44], G. A. Cowan[54], D. C. Craik[60], A. Crocombe[52], M. Cruz Torres[1], R. Currie[54], C. D'Ambrosio[44], F. Da Cunha Marinho[2], C. L. Da Silva[78], E. Dall'Occo[28], J. Dalseno[43,v], A. Danilina[35], A. Davis[3], O. De Aguiar Francisco[44], K. De Bruyn[44], S. De Capua[58], M. De Cian[45], J. M. De Miranda[1], L. De Paula[2], M. De Serio[15,d], P. De Simone[19], C.T. Dean[55], D. Decamp[5], L. Del Buono[9], B. Delaney[51], H.-P. Dembinski[12], M. Demmer[11], A. Dendek[31], D. Derkach[39], O. Deschamps[6], F. Desse[8], F. Dettori[56], B. Dey[69], A. Di Canto[44], P. Di Nezza[19], S. Didenko[74], H. Dijkstra[44], F. Dordei[44], M. Dorigo[44,y], A. Dosil Suárez[43], L. Douglas[55], A. Dovbnya[47], K. Dreimanis[56], L. Dufour[28], G. Dujany[9], P. Durante[44], J. M. Durham[78], D. Dutta[58], R. Dzhelyadin[41], M. Dziewiecki[13], A. Dziurda[30], A. Dzyuba[34], S. Easo[53], U. Egede[57], V. Egorychev[35], S. Eidelman[40,x], S. Eisenhardt[54], U. Eitschberger[11], R. Ekelhof[11], L. Eklund[55], S. Ely[63], A. Ene[33], S. Escher[10], S. Esen[28], T. Evans[61], A. Falabella[16], N. Farley[49], S. Farry[56], D. Fazzini[21,44,i], L. Federici[26], P. Fernandez Declara[44], A. Fernandez Prieto[43], F. Ferrari[16], L. Ferreira Lopes[45], F. Ferreira Rodrigues[2], M. Ferro-Luzzi[44], S. Filippov[37], R. A. Fini[15], M. Fiorini[17,g], M. Firlej[31], C. Fitzpatrick[45], T. Fiutowski[31], F. Fleuret[8,b], M. Fontana[44], F. Fontanelli[20,h], R. Forty[44], V. Franco Lima[56], M. Frank[44], C. Frei[44], J. Fu[22,q], W. Funk[44], C. Färber[44], M. Féo Pereira Rivello Carvalho[28], E. Gabriel[54], A. Gallas Torreira[43], D. Galli[16,e], S. Gallorini[24], S. Gambetta[54], Y. Gan[3], M. Gandelman[2], P. Gandini[22], Y. Gao[3], L. M. Garcia Martin[76], B. Garcia Plana[43], J. García Pardiñas[46], J. Garra Tico[51], L. Garrido[42], D. Gascon[42], C. Gaspar[44], L. Gavardi[11], G. Gazzoni[6], D. Gerick[13], E. Gersabeck[58], M. Gersabeck[58], T. Gershon[52], D. Gerstel[7], Ph. Ghez[5], V. Gibson[51], O. G. Girard[45], P. Gironella Gironell[42], L. Giubega[33], K. Gizdov[54], V. V. Gligorov[9], D. Golubkov[35], A. Golutvin[57,74], A. Gomes[1,a], I. V. Gorelov[36], C. Gotti[21,i], E. Govorkova[28], J. P. Grabowski[13], R. Graciani Diaz[42], L. A. Granado Cardoso[44], E. Graugés[42], E. Graverini[46], G. Graziani[18], A. Grecu[33], R. Greim[28], P. Griffith[23], L. Grillo[58], L. Gruber[44], B. R. Gruberg Cazon[59], O. Grünberg[71], C. Gu[3], E. Gushchin[37], A. Guth[10], Yu. Guz[41,44], T. Gys[44], C. Göbel[65], T. Hadavizadeh[59], C. Hadjivasiliou[6], G. Haefeli[45], C. Haen[44], S. C. Haines[51], B. Hamilton[62], X. Han[13], T. H. Hancock[59], S. Hansmann-Menzemer[13], N. Harnew[59], S. T. Harnew[50], T. Harrison[56], C. Hasse[44], M. Hatch[44], J. He[66], M. Hecker[57], K. Heinicke[11], A. Heister[11], K. Hennessy[56], L. Henry[76], E. van Herwijnen[44], J. Heuel[10], M. Heß[71], A. Hicheur[64], R. Hidalgo Charman[58], D. Hill[59], M. Hilton[58], P. H. Hopchev[45], J. Hu[13], W. Hu[69], W. Huang[66], Z. C. Huard[61], W. Hulsbergen[28], T. Humair[57], M. Hushchyn[39], D. Hutchcroft[56], D. Hynds[28], P. Ibis[11], M. Idzik[31], P. Ilten[49], K. Ivshin[34], R. Jacobsson[44], J. Jalocha[59], E. Jans[28], A. Jawahery[62], F. Jiang[3], M. John[59], D. Johnson[44], C. R. Jones[51], C. Joram[44], B. Jost[44], N. Jurik[59], S. Kandybei[47], M. Karacson[44], J. M. Kariuki[50], S. Karodia[55], N. Kazeev[39], M. Kecke[13], F. Keizer[51], M. Kelsey[63], M. Kenzie[51], T. Ketel[29], E. Khairullin[38], B. Khanji[44], C. Khurewathanakul[45], K. E. Kim[63], T. Kirn[10], S. Klaver[19], K. Klimaszewski[32], T. Klimkovich[12], S. Koliiev[48], M. Kolpin[13], R. Kopecna[13], P. Koppenburg[28], I. Kostiuk[28], S. Kotriakhova[34], M. Kozeiha[6], L. Kravchuk[37], M. Kreps[52], F. Kress[57], P. Krokovny[40,x], W. Krupa[31], W. Krzemien[32], W. Kucewicz[30,l], M. Kucharczyk[30], V. Kudryavtsev[40,x], A. K. Kuonen[45], T. Kvaratskheliya[35,44], D. Lacarrere[44], G. Lafferty[58], A. Lai[23], D. Lancierini[46], G. Lanfranchi[19], C. Langenbruch[10], T. Latham[52], C. Lazzeroni[49], R. Le Gac[7], A. Leflat[36], J. Lefrançois[8], R. Lefèvre[6], F. Lemaitre[44], O. Leroy[7], T. Lesiak[30], B. Leverington[13], P.-R. Li[66], Y. Li[4], Z. Li[63], X. Liang[63], T. Likhomanenko[73], R. Lindner[44], F. Lionetto[46], V. Lisovskyi[8], G. Liu[67], X. Liu[3], D. Loh[52], A. Loi[23], I. Longstaff[55], J. H. Lopes[2], G. H. Lovell[51], D. Lucchesi[24,o], M. Lucio Martinez[43], A. Lupato[24], E. Luppi[17,g], O. Lupton[44], A. Lusiani[25], X. Lyu[66], F. Machefert[8], F. Maciuc[33], V. Macko[45], P. Mackowiak[11], S. Maddrell-Mander[50], O. Maev[34,44], K. Maguire[58], D. Maisuzenko[34], M. W. Majewski[31], S. Malde[59], B. Malecki[30], A. Malinin[73], T. Maltsev[40,x], G. Manca[23,f], G. Mancinelli[7], D. Marangotto[22,q], J. Maratas[6,w], J. F. Marchand[5], U. Marconi[16], C. Marin Benito[8], M. Marinangeli[45], P. Marino[45], J. Marks[13], P. J. Marshall[56], G. Martellotti[27], M. Martin[7], M. Martinelli[44], D. Martinez Santos[43], F. Martinez Vidal[76], A. Massafferri[1], M. Materok[10], R. Matev[44], A. Mathad[52], Z. Mathe[44], C. Matteuzzi[21], A. Mauri[46], E. Maurice[8,b], B. Maurin[45], A. Mazurov[49], M. McCann[44,57], A. McNab[58], R. McNulty[14], J. V. Mead[56], B. Meadows[61], C. Meaux[7], N. Meinert[71], D. Melnychuk[32], M. Merk[28], A. Merli[22,q], E. Michielin[24], D. A. Milanes[70], E. Millard[52], M.-N. Minard[5], L. Minzoni[17,g], D. S. Mitzel[13], A. Mogini[9], R. D. Moise[57], T. Mombächer[11], I. A. Monroy[70], S. Monteil[6], M. Morandin[24], G. Morello[19], M. J. Morello[25,t], O. Morgunova[73], J. Moron[31], A. B. Morris[7], R. Mountain[63], F. Muheim[54], M. Mulder[28], C. H. Murphy[59], D. Murray[58], A. Mödden[11], D. Müller[44], J. Müller[11], K. Müller[46], V. Müller[11], P. Naik[50], T. Nakada[45], R. Nandakumar[53], A. Nandi[59], T. Nanut[45], I. Nasteva[2], M. Needham[54], N. Neri[22], S. Neubert[13], N. Neufeld[44], M. Neuner[13], R. Newcombe[57], T. D. Nguyen[45], C. Nguyen-Mau[45,n], S. Nieswand[10], R. Niet[11], N. Nikitin[36], A. Nogay[73], N. S. Nolte[44], D. P. O'Hanlon[16], A. Oblakowska-Mucha[31], V. Obraztsov[41], S. Ogilvy[19], R. Oldeman[23,f], C. J. G. Onderwater[72], A. Ossowska[30], J. M. Otalora Goicochea[2], T. Ovsiannikova[35], P. Owen[46], A. Oyanguren[76],

P. R. Pais[45], T. Pajero[25,t], A. Palano[15], M. Palutan[19], G. Panshin[75], A. Papanestis[53], M. Pappagallo[54], L. L. Pappalardo[17,g], W. Parker[62], C. Parkes[44,58], G. Passaleva[18,44], A. Pastore[15], M. Patel[57], C. Patrignani[16,e], A. Pearce[44], A. Pellegrino[28], G. Penso[27], M. Pepe Altarelli[44], S. Perazzini[44], D. Pereima[35], P. Perret[6], L. Pescatore[45], K. Petridis[50], A. Petrolini[20,h], A. Petrov[73], S. Petrucci[54], M. Petruzzo[22,q], B. Pietrzyk[5], G. Pietrzyk[45], M. Pikies[30], M. Pili[59], D. Pinci[27], J. Pinzino[44], F. Pisani[44], A. Piucci[13], V. Placinta[33], S. Playfer[54], J. Plews[49], M. Plo Casasus[43], F. Polci[9], M. Poli Lener[19], A. Poluektov[52], N. Polukhina[74,c], I. Polyakov[63], E. Polycarpo[2], G. J. Pomery[50], S. Ponce[44], A. Popov[41], D. Popov[12,49], S. Poslavskii[41], C. Potterat[2], E. Price[50], J. Prisciandaro[43], C. Prouve[50], V. Pugatch[48], A. Puig Navarro[46], H. Pullen[59], G. Punzi[25,p], W. Qian[66], J. Qin[66], R. Quagliani[9], B. Quintana[6], B. Rachwal[31], J. H. Rademacker[50], M. Rama[25], M. Ramos Pernas[43], M. S. Rangel[2], F. Ratnikov[38,39], G. Raven[29], M. Ravonel Salzgeber[44], M. Reboud[5], F. Redi[45], S. Reichert[11], A. C. dos Reis[1], F. Reiss[9], C. Remon Alepuz[76], Z. Ren[3], V. Renaudin[8], S. Ricciardi[53], S. Richards[50], K. Rinnert[56], P. Robbe[8], A. Robert[9], A. B. Rodrigues[45], E. Rodrigues[61], J. A. Rodriguez Lopez[70], M. Roehrken[44], S. Roiser[44], A. Rollings[59], V. Romanovskiy[41], A. Romero Vidal[43], M. Rotondo[19], M. S. Rudolph[63], T. Ruf[44], J. Ruiz Vidal[76], J. J. Saborido Silva[43], N. Sagidova[34], B. Saitta[23,f], V. Salustino Guimaraes[65], C. Sanchez Gras[28], C. Sanchez Mayordomo[76], B. Sanmartin Sedes[43], R. Santacesaria[27], C. Santamarina Rios[43], M. Santimaria[19,44], E. Santovetti[26,j], G. Sarpis[58], A. Sarti[19,k], C. Satriano[27,s], A. Satta[26], M. Saur[66], D. Savrina[35,36], S. Schael[10], M. Schellenberg[11], M. Schiller[55], H. Schindler[44], M. Schmelling[12], T. Schmelzer[11], B. Schmidt[44], O. Schneider[45], A. Schopper[44], H. F. Schreiner[61], M. Schubiger[45], M. H. Schune[8], R. Schwemmer[44], B. Sciascia[19], A. Sciubba[27,k], A. Semennikov[35], E. S. Sepulveda[9], A. Sergi[44,49], N. Serra[46], J. Serrano[7], L. Sestini[24], A. Seuthe[11], P. Seyfert[44], M. Shapkin[41], Y. Shcheglov[34,†], T. Shears[56], L. Shekhtman[40,x], V. Shevchenko[73], E. Shmanin[74], B. G. Siddi[17], R. Silva Coutinho[46], L. Silva de Oliveira[2], G. Simi[24,o], S. Simone[15,d], I. Skiba[17], N. Skidmore[13], T. Skwarnicki[63], M. W. Slater[49], J. G. Smeaton[51], E. Smith[10], I. T. Smith[54], M. Smith[57], M. Soares[16], l. Soares Lavra[1], M. D. Sokoloff[61], F. J. P. Soler[55], B. Souza De Paula[2], B. Spaan[11], E. Spadaro Norella[22,q], P. Spradlin[55], F. Stagni[44], M. Stahl[13], S. Stahl[44], P. Stefko[45], S. Stefkova[57], O. Steinkamp[46], S. Stemmle[13], O. Stenyakin[41], M. Stepanova[34], H. Stevens[11], A. Stocchi[8], S. Stone[63], B. Storaci[46], S. Stracka[25], M. E. Stramaglia[45], M. Straticiuc[33], U. Straumann[46], S. Strokov[75], J. Sun[3], L. Sun[68], K. Swientek[31], A. Szabelski[32], T. Szumlak[31], M. Szymanski[66], S. T'Jampens[5], Z. Tang[3], A. Tayduganov[7], T. Tekampe[11], G. Tellarini[17], F. Teubert[44], E. Thomas[44], J. van Tilburg[28], M. J. Tilley[57], V. Tisserand[6], M. Tobin[31], S. Tolk[44], L. Tomassetti[17,g], D. Tonelli[25], D. Y. Tou[9], R. Tourinho Jadallah Aoude[1], E. Tournefier[5], M. Traill[55], M. T. Tran[45], A. Trisovic[51], A. Tsaregorodtsev[7], G. Tuci[25,p], A. Tully[51], N. Tuning[28,44], A. Ukleja[32], A. Usachov[8], A. Ustyuzhanin[38], U. Uwer[13], A. Vagner[75], V. Vagnoni[16], A. Valassi[44], S. Valat[44], G. Valenti[16], R. Vazquez Gomez[44], P. Vazquez Regueiro[43], S. Vecchi[17], M. van Veghel[28], J. J. Velthuis[50], M. Veltri[18,r], G. Veneziano[59], A. Venkateswaran[63], M. Vernet[6], M. Veronesi[28], N. V. Veronika[14], M. Vesterinen[59], J. V. Viana Barbosa[44], D. Vieira[66], M. Vieites Diaz[43], H. Viemann[71], X. Vilasis-Cardona[42,m], A. Vitkovskiy[28], M. Vitti[51], V. Volkov[36], A. Vollhardt[46], D. Vom Bruch[9], B. Voneki[44], A. Vorobyev[34], V. Vorobyev[40,x], J. A. de Vries[28], C. Vázquez Sierra[28], R. Waldi[71], J. Walsh[25], J. Wang[4], M. Wang[3], Y. Wang[69], Z. Wang[46], D. R. Ward[51], H. M. Wark[56], N. K. Watson[49], D. Websdale[57], A. Weiden[46], C. Weisser[60], M. Whitehead[10], J. Wicht[52], G. Wilkinson[59], M. Wilkinson[63], I. Williams[51], M. R. J. Williams[58], M. Williams[60], T. Williams[49], F. F. Wilson[53], M. Winn[8], W. Wislicki[32], M. Witek[30], G. Wormser[8], S. A. Wotton[51], K. Wyllie[44], D. Xiao[69], Y. Xie[69], A. Xu[3], M. Xu[69], Q. Xu[66], Z. Xu[3], Z. Xu[5], Z. Yang[3], Z. Yang[62], Y. Yao[63], L. E. Yeomans[56], H. Yin[69], J. Yu[69,aa], X. Yuan[63], O. Yushchenko[41], K. A. Zarebski[49], M. Zavertyaev[12,c], D. Zhang[69], L. Zhang[3], W. C. Zhang[3,z], Y. Zhang[8], A. Zhelezov[13], Y. Zheng[66], X. Zhu[3], V. Zhukov[10,36], J. B. Zonneveld[54], S. Zucchelli[16]

[1] Centro Brasileiro de Pesquisas Físicas (CBPF), Rio de Janeiro, Brazil
[2] Universidade Federal do Rio de Janeiro (UFRJ), Rio de Janeiro, Brazil
[3] Center for High Energy Physics, Tsinghua University, Beijing, China
[4] Institute Of High Energy Physics (ihep), Beijing, China
[5] Université Grenoble Alpes, Université Savoie Mont Blanc, CNRS, IN2P3-LAPP, Annecy, France
[6] Clermont Université, Université Blaise Pascal, CNRS/IN2P3, LPC, Clermont-Ferrand, France
[7] Aix-Marseille Univ, CNRS/IN2P3, CPPM, Marseille, France
[8] LAL, Univ. Paris-Sud, CNRS/IN2P3, Université Paris-Saclay, Orsay, France
[9] LPNHE, Sorbonne Université, Paris Diderot Sorbonne Paris Cité, CNRS/IN2P3, Paris, France
[10] I. Physikalisches Institut, RWTH Aachen University, Aachen, Germany
[11] Fakultät Physik, Technische Universität Dortmund, Dortmund, Germany
[12] Max-Planck-Institut für Kernphysik (MPIK), Heidelberg, Germany
[13] Physikalisches Institut, Ruprecht-Karls-Universität Heidelberg, Heidelberg, Germany

[14] School of Physics, University College Dublin, Dublin, Ireland
[15] INFN Sezione di Bari, Bari, Italy
[16] INFN Sezione di Bologna, Bologna, Italy
[17] INFN Sezione di Ferrara, Ferrara, Italy
[18] INFN Sezione di Firenze, Florence, Italy
[19] INFN Laboratori Nazionali di Frascati, Frascati, Italy
[20] INFN Sezione di Genova, Genova, Italy
[21] INFN Sezione di Milano-Bicocca, Milan, Italy
[22] INFN Sezione di Milano, Milan, Italy
[23] INFN Sezione di Cagliari, Monserrato, Italy
[24] INFN Sezione di Padova, Padua, Italy
[25] INFN Sezione di Pisa, Pisa, Italy
[26] INFN Sezione di Roma Tor Vergata, Rom, Italy
[27] INFN Sezione di Roma La Sapienza, Rom, Italy
[28] Nikhef National Institute for Subatomic Physics, Amsterdam, The Netherlands
[29] Nikhef National Institute for Subatomic Physics and VU University Amsterdam, Amsterdam, The Netherlands
[30] Henryk Niewodniczanski Institute of Nuclear Physics Polish Academy of Sciences, Kraków, Poland
[31] Faculty of Physics and Applied Computer Science, AGH-University of Science and Technology, Kraków, Poland
[32] National Center for Nuclear Research (NCBJ), Warsaw, Poland
[33] Horia Hulubei National Institute of Physics and Nuclear Engineering, Bucharest-Magurele, Romania
[34] Petersburg Nuclear Physics Institute (PNPI), Gatchina, Russia
[35] Institute of Theoretical and Experimental Physics (ITEP), Moscow, Russia
[36] Institute of Nuclear Physics, Moscow State University (SINP MSU), Moscow, Russia
[37] Institute for Nuclear Research of the Russian Academy of Sciences (INR RAS), Moscow, Russia
[38] Yandex School of Data Analysis, Moscow, Russia
[39] National Research University Higher School of Economics, Moscow, Russia
[40] Budker Institute of Nuclear Physics (SB RAS), Novosibirsk, Russia
[41] Institute for High Energy Physics (IHEP), Protvino, Russia
[42] ICCUB, Universitat de Barcelona, Barcelona, Spain
[43] Instituto Galego de Física de Altas Enerxías (IGFAE), Universidade de Santiago de Compostela, Santiago de Compostela, Spain
[44] European Organization for Nuclear Research (CERN), Geneva, Switzerland
[45] Institute of Physics, Ecole Polytechnique Fédérale de Lausanne (EPFL), Lausanne, Switzerland
[46] Physik-Institut, Universität Zürich, Zürich, Switzerland
[47] NSC Kharkiv Institute of Physics and Technology (NSC KIPT), Kharkiv, Ukraine
[48] Institute for Nuclear Research of the National Academy of Sciences (KINR), Kyiv, Ukraine
[49] University of Birmingham, Birmingham, UK
[50] H.H. Wills Physics Laboratory, University of Bristol, Bristol, UK
[51] Cavendish Laboratory, University of Cambridge, Cambridge, UK
[52] Department of Physics, University of Warwick, Coventry, UK
[53] STFC Rutherford Appleton Laboratory, Didcot, UK
[54] School of Physics and Astronomy, University of Edinburgh, Edinburgh, UK
[55] School of Physics and Astronomy, University of Glasgow, Glasgow, UK
[56] Oliver Lodge Laboratory, University of Liverpool, Liverpool, UK
[57] Imperial College London, London, UK
[58] School of Physics and Astronomy, University of Manchester, Manchester, UK
[59] Department of Physics, University of Oxford, Oxford, UK
[60] Massachusetts Institute of Technology, Cambridge, MA, USA
[61] University of Cincinnati, Cincinnati, OH, USA
[62] University of Maryland, College Park, MD, USA
[63] Syracuse University, Syracuse, NY, USA
[64] Laboratory of Mathematical and Subatomic Physics, Constantine, Algeria, associated to[2]
[65] Pontifícia Universidade Católica do Rio de Janeiro (PUC-Rio), Rio de Janeiro, Brazil, associated to[2]

[66] University of Chinese Academy of Sciences, Beijing, China, associated to[3]
[67] South China Normal University, Guangzhou, China, associated to[3]
[68] School of Physics and Technology, Wuhan University, Wuhan, China, associated to[3]
[69] Institute of Particle Physics, Central China Normal University, Wuhan, Hubei, China, associated to[3]
[70] Departamento de Fisica, Universidad Nacional de Colombia, Bogota, Colombia, associated to[9]
[71] Institut für Physik, Universität Rostock, Rostock, Germany, associated to[13]
[72] Van Swinderen Institute, University of Groningen, Groningen, The Netherlands, associated to[28]
[73] National Research Centre Kurchatov Institute, Moscow, Russia, associated to[35]
[74] National University of Science and Technology "MISIS", Moscow, Russia, associated to[35]
[75] National Research Tomsk Polytechnic University, Tomsk, Russia, associated to[35]
[76] Instituto de Fisica Corpuscular, Centro Mixto Universidad de Valencia-CSIC, Valencia, Spain, associated to[42]
[77] University of Michigan, Ann Arbor, USA, associated to[63]
[78] Los Alamos National Laboratory (LANL), Los Alamos, USA, associated to[63]

[a] Universidade Federal do Triângulo Mineiro (UFTM), Uberaba-MG, Brazil
[b] Laboratoire Leprince-Ringuet, Palaiseau, France
[c] P.N. Lebedev Physical Institute, Russian Academy of Science (LPI RAS), Moscow, Russia
[d] Università di Bari, Bari, Italy
[e] Università di Bologna, Bologna, Italy
[f] Università di Cagliari, Cagliari, Italy
[g] Università di Ferrara, Ferrara, Italy
[h] Università di Genova, Genova, Italy
[i] Università di Milano Bicocca, Milan, Italy
[j] Università di Roma Tor Vergata, Rom, Italy
[k] Università di Roma La Sapienza, Rom, Italy
[l] AGH-University of Science and Technology, Faculty of Computer Science, Electronics and Telecommunications, Kraków, Poland
[m] LIFAELS, La Salle, Universitat Ramon Llull, Barcelona, Spain
[n] Hanoi University of Science, Hanoi, Vietnam
[o] Università di Padova, PadUA, Italy
[p] Università di Pisa, Pisa, Italy
[q] Università degli Studi di Milano, Milan, Italy
[r] Università di Urbino, Urbino, Italy
[s] Università della Basilicata, Potenza, Italy
[t] Scuola Normale Superiore, Pisa, Italy
[u] Università di Modena e Reggio Emilia, Modena, Italy
[v] H.H. Wills Physics Laboratory, University of Bristol, Bristol, UK
[w] MSU - Iligan Institute of Technology (MSU-IIT), Iligan, Philippines
[x] Novosibirsk State University, Novosibirsk, Russia
[y] Sezione INFN di Trieste, Trieste, Italy
[z] School of Physics and Information Technology, Shaanxi Normal University (SNNU), Xi'an, China
[aa] Physics and Micro Electronic College, Hunan University, Changsha City, China
[†] Deceased